

# Metal-dielectric-metal plasmonic waveguide devices for manipulating light at the nanoscale

Invited Paper

Georgios Veronis<sup>1\*</sup>, Zongfu Yu<sup>2</sup>, Şükrü Ekin Kocabaş<sup>2</sup>, David A. B. Miller<sup>2</sup>,  
Mark L. Brongersma<sup>3</sup>, and Shanhui Fan<sup>2</sup>

<sup>1</sup>Department of Electrical and Computer Engineering and Center for Computation  
and Technology, Louisiana State University, Baton Rouge, LA 70803, USA

<sup>2</sup>Ginzton Laboratory, Stanford University, Stanford, CA 94305, USA

<sup>3</sup>Geballe Laboratory of Advanced Materials, Stanford University, Stanford, CA 94305, USA

\*E-mail: gveronis@lsu.edu

Received December 23, 2008

We review some of the recent advances in the development of subwavelength plasmonic devices for manipulating light at the nanoscale, drawing examples from our own work in metal-dielectric-metal (MDM) plasmonic waveguide devices. We introduce bends, splitters, and mode converters for MDM waveguides with no additional loss. We also demonstrate that optical gain provides a mechanism for on/off switching in MDM plasmonic waveguides. Highly efficient compact couplers between dielectric waveguides and MDM waveguides are also introduced.

OCIS codes: 130.2790, 240.6680, 260.2110.

doi: 10.3788/COL20090704.0302.

## 1. Introduction

Light-guiding structures which allow subwavelength confinement of the optical mode are important for achieving compact integrated photonic devices<sup>[1–7]</sup>. The minimum confinement of a guided optical mode in dielectric waveguides is set by the diffraction limit and is of the order of  $\lambda_0/n$ , where  $\lambda_0$  is the wavelength in free space and  $n$  is the refractive index. As opposed to dielectric waveguides, plasmonic waveguides have shown the potential to guide subwavelength optical modes, the so-called surface plasmon polaritons, at metal-dielectric interfaces.

Several different plasmonic waveguiding structures have been proposed, such as metallic nanowires<sup>[2,3]</sup> and metallic nanoparticle arrays<sup>[4,5]</sup>. Most of these structures support a highly-confined mode only near the surface plasmon frequency. In this regime, the optical mode typically has low group velocity and short propagation length. It has been shown however that a metal-dielectric-metal (MDM) structure with a dielectric region thickness of  $\sim 100$  nm supports a propagating mode with a nanoscale modal size at a wavelength range extending from zero-frequency (DC) to visible<sup>[8]</sup>. Thus, such a waveguide could be potentially important in providing an interface between conventional optics and subwavelength electronic and optoelectronic devices. Because of the predicted attractive properties of MDM waveguides, their modal structure has been studied in great detail<sup>[8–12]</sup>, and people have also started to explore such structures experimentally<sup>[13–15]</sup>. Recent research work has therefore focused on the development of functional plasmonic devices, including active devices, for nanoscale plasmonic integrated circuits.

Here we provide a review of some of our own recent research activities aiming to advance the state of the art of plasmonics through the introduction of novel MDM plas-

monic waveguide devices for manipulating light at the nanoscale<sup>[16–19]</sup>. We first briefly review the simulation method used in our studies, then introduce bends, splitters, and mode converters for MDM waveguides with no additional loss. We also demonstrate that optical gain provides a mechanism for on/off switching in MDM plasmonic waveguides. Finally, we introduce highly efficient compact couplers between dielectric waveguides and MDM waveguides.

## 2. Simulation method

We study the properties of MDM plasmonic waveguide devices using a two-dimensional (2D) finite-difference frequency-domain (FDFD) method<sup>[20,21]</sup>. This method allows us to directly use experimental data for the frequency-dependent dielectric constant of metals such as silver<sup>[22]</sup>, including both the real and imaginary parts, with no further approximation. Perfectly matched layer (PML) absorbing boundary conditions are used at all boundaries of the simulation domain<sup>[23]</sup>.

Due to the rapid field variation at the metal-dielectric interfaces, a very fine grid resolution of  $\sim 1$  nm is required at the metal-dielectric interfaces to adequately resolve the local fields. On the other hand, a grid resolution of  $\sim \lambda/20$  is sufficient in other regions of the simulation domain. For example, the required grid size in air at  $\lambda_0 = 1.55 \mu\text{m}$  is  $\sim 77.5$  nm, which is almost two orders of magnitude larger than the required grid size at the metal-dielectric interfaces. We therefore use a nonuniform orthogonal grid<sup>[24]</sup> to avoid an unnecessary computational cost. We found that by using such a grid our results are accurate to  $\sim 0.05\%$ .

## 3. Bends and splitters

In this section, we investigate the performance of bends and power splitters in MDM plasmonic wave-

uities. Waveguide bends and splitters are basic structures for optical interconnects and therefore essential components of optical integrated circuits<sup>[6,25]</sup>. Here, the relevant question is whether MDM bends and splitters will induce reflection or excess absorption loss on top of the propagation loss in the waveguides.

To answer this question, we calculate the transmission coefficient of bends and splitters and normalize it with respect to the transmission coefficient of a straight waveguide with the same length. In all cases, the waveguide width  $d$  is much smaller than the wavelength so that only the fundamental TM waveguide mode (with magnetic field perpendicular to the direction of propagation) is excited. In Fig. 1, we show the calculated power transmission coefficient of a 90° sharp MDM waveguide bend (inset of Fig. 1) as a function of wavelength. We observe that there is no bending loss in a broad wavelength range that extends from DC to near-infrared. This range includes the optical communication wavelength of 1.55  $\mu\text{m}$ .

To explain the absence of bending loss in subwavelength MDM bends, we introduce an effective characteristic impedance model based upon the dispersion relation of the MDM waveguide structures. The characteristic impedance of the fundamental TEM mode in a perfect electric conductor (PEC) parallel-plate waveguide is uniquely defined as the ratio of voltage  $V$  to surface current density  $I$  and is equal to<sup>[26]</sup>

$$Z_{\text{TEM}} \equiv \frac{V}{I} = \frac{E_x d}{H_y} = \frac{\beta_{\text{TEM}}}{\omega \epsilon_0} d = \sqrt{\frac{\mu_0}{\epsilon_0}} d, \quad (1)$$

where  $E_x, H_y$  are the transverse components of the electric and magnetic fields, respectively, and we assumed a unit-length waveguide in the  $y$  direction. For non-TEM modes, such as the fundamental MDM mode, voltage and current are not uniquely defined. However, metals like silver satisfy the condition  $|\epsilon_{\text{metal}}| \gg \epsilon_{\text{diel}}$  at the optical communication wavelength of 1.55  $\mu\text{m}$ <sup>[22]</sup>. Thus,  $|E_{x \text{ metal}}| \ll |E_{x \text{ diel}}|$ , so that the integral of the electric field in the transverse direction can be approximated by  $E_{x \text{ diel}} d$  and we may therefore define the characteristic impedance of the fundamental MDM mode as

$$Z_{\text{MDM}}(d) \equiv \frac{E_{x \text{ diel}} d}{H_y \text{ diel}} = \frac{\beta_{\text{MDM}}(d)}{\omega \epsilon_0} d, \quad (2)$$

where  $\beta_{\text{MDM}}(d) = 2\pi/\lambda_g(d)$  is the real part of the mode propagation constant<sup>[26]</sup>, and  $\lambda_g$  is the guide wavelength

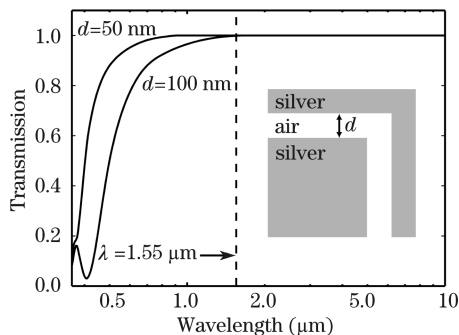


Fig. 1. Power transmission spectra of a MDM waveguide bend (shown in the inset) calculated using FDFD.

of the fundamental TM mode in the MDM waveguide, which is smaller than the free-space wavelength  $\lambda_0$ <sup>[8]</sup>.

In the case of a MDM bend, if the structure dimensions are small in comparison with the wavelength, the quasistatic approximation holds<sup>[26]</sup>. Under the quasistatic approximation, the bend is equivalent to a junction between two transmission lines with the same characteristic impedance, and there is therefore no bending loss. The limiting wavelength  $\lambda_c$  at which the transmission coefficient decreases below 99% is 1.27  $\mu\text{m}$  (0.76  $\mu\text{m}$ ) for  $d = 100$  nm ( $d = 50$  nm) (Fig. 1). The operating wavelength range widens as  $d$  decreases, because for thinner structures the quasistatic approximation holds over a wider range of wavelengths.

We also calculate the transmission spectra of MDM splitters (inset of Fig. 2). The frequency response of MDM splitters is quite similar to the response of MDM bends. At long wavelengths the transmission is equal to 44.4% for  $d_{\text{in}} = d_{\text{out}}$ . Under the quasistatic approximation, which holds at long wavelengths, the splitter is equivalent to a junction of three transmission lines with the same characteristic impedance  $Z_0$ . The load connected to the input transmission line at the junction consists of the series combination of the two output transmission lines. Thus, the equivalent load impedance is  $Z_L = 2Z_0$  and the reflection coefficient is  $\bar{R} = |(Z_L - Z_0)/(Z_L + Z_0)|^2 = 1/9$ . Because of the symmetry of the structure, the transmitted optical power is equally distributed between the two output waveguide branches, so that the transmission coefficient is  $T = 4/9 = 44.4\%$ .

Based on the above discussion, in order to improve the transmission coefficient of the MDM splitter, we can adjust the characteristic impedance of the input waveguide  $Z_{\text{in}}$  so that  $Z_{\text{in}} \simeq Z_L = 2Z_0$ . The input impedance  $Z_{\text{in}}$  can be adjusted by varying the thickness  $d_{\text{in}}$  of the input waveguide. In Fig. 2, we show the calculated reflection coefficient  $R$  of the MDM T-shaped splitter at  $\lambda_0 = 1.55$   $\mu\text{m}$  as a function of  $d_{\text{in}}/d_{\text{out}}$ , for  $d_{\text{out}} = 50$  nm (inset of Fig. 2). We note that at  $\lambda_0 = 1.55$   $\mu\text{m}$  the propagation length of the fundamental MDM mode is much larger than the splitter dimensions so that the contribution of excess absorption to the splitter loss is negligible. We observe that the

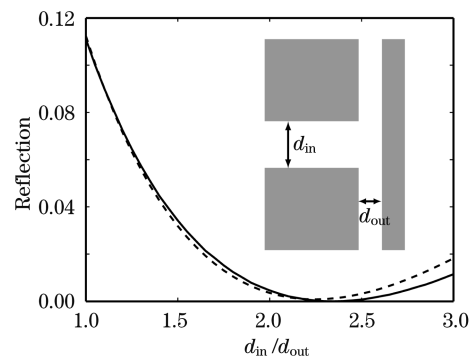


Fig. 2. Reflection coefficient  $R$  of a MDM T-shaped splitter (shown in the inset) as a function of  $d_{\text{in}}/d_{\text{out}}$  at  $\lambda_0 = 1.55$   $\mu\text{m}$  calculated using FDFD. We also show with dashed line the reflection coefficient  $\bar{R}$  calculated based on the characteristic impedance  $Z_{\text{MDM}}$  and transmission-line theory. Results are shown for  $d_{\text{out}} = 50$  nm.

reflection coefficient is below 1% for  $1.8 < d_{\text{in}}/d_{\text{out}} < 2.8$  and is minimized for  $d_{\text{in}}/d_{\text{out}} \simeq 2.25$ . In Fig. 2, we also show the reflection coefficient of the MDM T-shaped splitter calculated based on  $Z_{\text{MDM}}$  as

$$\bar{R} = \left| \frac{Z_L - Z_0}{Z_L + Z_0} \right|^2 = \left| \frac{2Z_{\text{MDM}}(d_{\text{out}}) - Z_{\text{MDM}}(d_{\text{in}})}{2Z_{\text{MDM}}(d_{\text{out}}) + Z_{\text{MDM}}(d_{\text{in}})} \right|^2. \quad (3)$$

We observe that there is a very good agreement between  $\bar{R}$  and the exact reflection coefficient  $R$  calculated using FDFD. This agreement suggests that the concept of characteristic impedance for MDM waveguides is indeed valid and useful. The deviation between  $\bar{R}$  and  $R$  at large values of  $d_{\text{in}}/d_{\text{out}}$  is due to the fact that  $d_{\text{in}}$  is not very small compared with the wavelength and the quasistatic approximation therefore breaks down. Similar deviations are observed for PEC parallel-plate waveguides. Such deviations decrease at longer wavelengths in both the PEC and MDM waveguide cases.

#### 4. Mode converters

In this section, we investigate the performance of mode converters which couple efficiently the modes of two MDM plasmonic waveguides with different widths. Mode converters can act as impedance matching circuits maximizing the coupling between plasmonic waveguides and optoelectronic devices, and will therefore be essential components of plasmonic integrated circuits.

Here we design a mode converter to couple the mode of a wavelength-sized MDM waveguide to that of a sub-wavelength one. Since the quasistatic approximation does not hold for wavelength-sized components, we use a more general scattering matrix formalism instead of the characteristic impedance model.

We first consider the junction between two MDM plasmonic waveguides with different widths which both support a single propagating mode. In such a case, far away from the waveguide junction the fields can be written in terms of this fundamental mode of the system, since all higher order modes will have an exponential decay much faster compared with the main propagating mode. Under such circumstances, the effects of the waveguide junction on the propagating modes can be described using the single mode scattering matrix ( $\mathbf{S}$ ) formalism<sup>[27]</sup>. The scattering matrix relates the transverse magnetic field of the modes that arrive at the left and right ports,  $H_L^+$ ,  $H_R^+$  to the transverse magnetic field of the modes that propagate away from the ports,  $H_L^-$  and  $H_R^-$ :

$$\begin{pmatrix} H_L^- \\ H_R^- \end{pmatrix} = \begin{pmatrix} S_{11} & S_{12} \\ S_{21} & S_{22} \end{pmatrix} \begin{pmatrix} H_L^+ \\ H_R^+ \end{pmatrix}. \quad (4)$$

Here, we design a mode converter consisting of a cascade connection of two junctions (inset of Fig. 3(b)) to minimize the reflection at a specific frequency. Such a structure can be modeled as two junctions with scattering matrices,  ${}^L\mathbf{S}$  and  ${}^R\mathbf{S}$ , separated by a center waveguide of length  $l$  as shown in Fig. 3(a). When different scattering matrices are cascaded, the transfer matrix,  $\mathbf{T}$ , leads to a much simpler formulation<sup>[28]</sup>

$$\begin{pmatrix} H_L^+ \\ H_L^- \end{pmatrix} = \begin{pmatrix} T_{11} & T_{12} \\ T_{21} & T_{22} \end{pmatrix} \begin{pmatrix} H_R^- \\ H_R^+ \end{pmatrix}. \quad (5)$$

In order to have zero reflection ( $H_L^- = 0$ ), one should have  $T_{21}H_R^- + T_{22}H_R^+ = 0$ , which can be cast in terms of the scattering parameters as

$$S_{11}H_R^- = (S_{11}S_{22} - S_{12}S_{21})H_R^+. \quad (6)$$

If the mode that propagates toward the right junction has unit strength at its input plane, we have  $H_C^- = e^{ik_C l}$  and  $H_C^+ = {}^R S_{11} e^{-ik_C l}$ , where  $k_C$  is the wave vector of the center waveguide. With these definitions, the condition for zero reflection, Eq. (6), for the left junction can be written as

$$e^{-2ik_C l} = \frac{{}^L S_{11} / {}^R S_{11}}{{}^L S_{11} {}^L S_{22} - {}^L S_{21}^2}, \quad (7)$$

where we also use the fact that for reciprocal media  $S_{12} = S_{21}$ .

If the system were lossless, then the scattering matrix would be unitary ( $\mathbf{S}\mathbf{S}^\dagger = 1$ ), which implies the following conditions:

$$\begin{aligned} |S_{11}|^2 &= |S_{22}|^2 = 1 - |S_{12}|^2, \\ \frac{S_{12}}{S_{21}} &= -\frac{S_{22}}{S_{11}^*}. \end{aligned} \quad (8)$$

Using (7) and (8), the zero reflection condition becomes

$$\begin{aligned} |{}^L S_{22}| &= |{}^R S_{11}|, \\ \angle {}^L S_{22} + \angle {}^R S_{11} &= 2k_C l + 2\pi n, \end{aligned} \quad (10)$$

where  $n$  is any integer value. This means that to match a left waveguide to a right waveguide, one should choose a center waveguide width which satisfies Eq. (9), and decide on the length of the center waveguide based on Eq. (10). Once a matching left, center and right waveguide triplet is found, the procedure can be recursively repeated to cascade more junctions without getting any reflection at the leftmost waveguide.

We can use the conditions (7), (9), and (10) for zero reflection, to design the mode converter. Condition (7) is more general and applicable to the lossy case. We extracted  $\mathbf{S}$  for the lossless metal case. The results were very similar to the case where the loss was included. That led us to suspect that the conditions for the lossless reciprocal junctions, (9) and (10), would be essentially sufficient in the design of a mode converter that converts the mode of a wavelength-sized MDM waveguide ( $d = 0.9\lambda_0$ ) to that of a subwavelength one with no reflection.

In our design, we choose the left waveguide width to be  $0.9\lambda_0$  and the center waveguide width to be  $0.5\lambda_0$ , as shown in the inset in Fig. 3(b). The parameters that we need are the insulator width of the right waveguide,  $w$ , and the length of the center waveguide,  $l$ .

The width of the right waveguide can be chosen by satisfying (9) ( $|{}^L S_{22}| = |{}^R S_{11}|$ ). We find that this corresponds to a right waveguide thickness of  $0.16\lambda_0$ . The phase condition (10) then gives, after some simplification through the use of the numerical value for  $k_C$ ,  $l/\lambda_0 = 0.1377 + 0.4861n$ .

To check our design, we calculated the reflection coefficient for the structure shown in the inset of Fig. 3(b) using FDFD. We also calculated the reflection coefficient through the use of the transfer matrix formalism in which we multiplied the transfer matrices for

the right junction,  $\mathbf{T}_R$ , a center waveguide of length  $l$ ,  $\mathbf{T}_C$ , and the left junction,  $\mathbf{T}_L$ , to get the overall transfer matrix  $\mathbf{T} = \mathbf{T}_L \mathbf{T}_C \mathbf{T}_R$ . We did the calculations for two different sets of  $\{\mathbf{T}_R, \mathbf{T}_L\}$ : one in which we used the scattering matrices for the lossy junctions and another for the lossless junctions. The center waveguide of length  $l$  had loss in both cases, i.e.,  $k_C = (1.03 - i9.45 \times 10^{-4})2\pi/\lambda_0$ .

Figure 3(b) verifies that lossless junction models are quite effective at modeling the waveguide discontinuities and the prediction of the length of the center guide for zero reflection reached by their use,  $l/\lambda_0 = 0.1377 + 0.4861n$ , is very accurate. The lossy junction model on the other hand gives results essentially indistinguishable from the simulation results as long as the two junctions are not very close to each other ( $< 0.1\lambda_0$ ). When the junctions get very close, the coupling of higher order non-propagating modes becomes important and the single mode modeling we employed in the construction of scattering matrices breaks down. For such closely spaced junctions, the whole structure should be treated as a single unit.

### 5. Gain-induced switches

In the previous sections, we have shown that passive MDM plasmonic waveguide devices can efficiently manipulate light at the nanoscale. Another essential component of optical integrated circuits is devices, such as optical switches, that enable active light manipulation. In this section, we demonstrate that optical gain provides a mechanism for on/off switching in MDM plasmonic waveguides. Previously, the use of media with optical gain has been suggested as a means to compensate for the material loss in the metal<sup>[29–35]</sup>, to increase the resolution of negative-refractive-index near-field lenses<sup>[36]</sup>, and to control the group velocity of nanoscale plasmonic waveguides<sup>[37]</sup>.

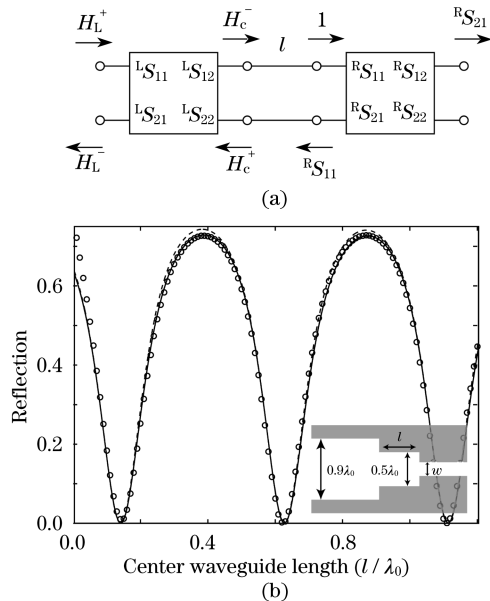


Fig. 3. (a) Schematic diagram of modal propagation. The left and right junctions are shown as boxes with an  $\mathbf{S}$  matrix description. The center waveguide is shown as a transmission line of length  $l$ . (b) Reflection coefficient for  $w = 0.16\lambda_0$  as a function of  $l/\lambda_0$  at  $\lambda_0 = 1.55 \mu\text{m}$  calculated using FDFD (circles). Transfer matrix calculations using lossy (solid line) and lossless (dashed line) junction models are also plotted.

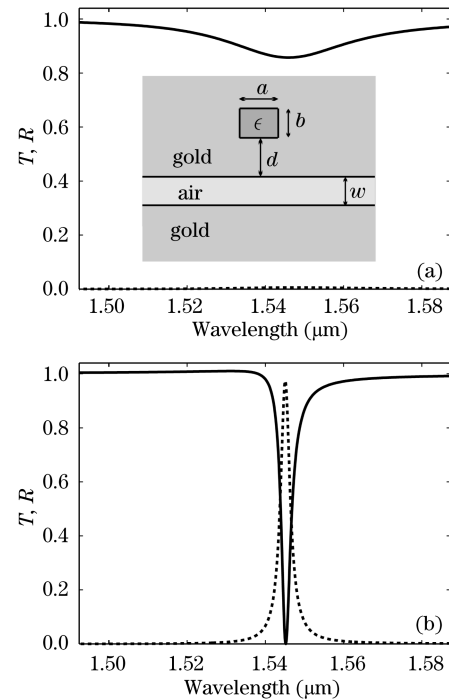


Fig. 4. (a) Transmission  $T$  (solid line) and reflection  $R$  (dashed line) spectra of a gold-air-gold MDM plasmonic waveguide side-coupled to a rectangular cavity (shown in the inset) calculated using FDFD. Results are shown for  $w = 50 \text{ nm}$ ,  $d = 100 \text{ nm}$ ,  $a = 200 \text{ nm}$ , and  $b = 280 \text{ nm}$ . The cavity is filled with InGaAsP, and there is no pumping of InGaAsP ( $\epsilon = 11.38 - i0.1$ ). (b) Same as (a), except that there is pumping of InGaAsP ( $\epsilon = 11.38 + i0.165$ ).

We consider a subwavelength gold-air-gold MDM plasmonic waveguide side-coupled to a rectangular cavity<sup>[38,39]</sup> filled with an InGaAsP semiconductor gain medium with dielectric permittivity  $\epsilon = 11.38 + i\epsilon_i$  (inset of Fig. 4(a)).

Such a system consisting of a waveguide side-coupled to a cavity, which supports a resonant mode of frequency  $\omega_0$ , can be described using a temporal coupled-mode theory<sup>[40]</sup>. Using coupled-mode theory it can be shown that the transmission coefficient  $T$  and reflection coefficient  $R$  of the system are given by<sup>[40]</sup>

$$T = \frac{(\omega - \omega_0)^2 + (\frac{1}{\tau_0} - \frac{1}{\tau_g})^2}{(\omega - \omega_0)^2 + (\frac{1}{\tau_0} - \frac{1}{\tau_g} + \frac{1}{\tau_e})^2}, \quad (11)$$

$$R = \frac{(\frac{1}{\tau_e})^2}{(\omega - \omega_0)^2 + (\frac{1}{\tau_0} - \frac{1}{\tau_g} + \frac{1}{\tau_e})^2}, \quad (12)$$

where  $\omega$  is the frequency,  $1/\tau_e$  is the decay rate of the field in the cavity due to the power escape through the waveguide,  $1/\tau_0$  is the decay rate of the field due to the material loss in the metal, and  $1/\tau_g$  is the growth rate of the field due to the gain of the material in the cavity. We observe that far from the resonant frequency  $\omega_0$ , the cavity mode is not excited, and the incident waveguide mode is completely transmitted. In addition, we observe that when  $1/\tau_0 - 1/\tau_g \gg 1/\tau_e$ , there is very low reflection and high transmission at resonance. In contrast, when  $1/\tau_0 = 1/\tau_g$ , the decay of the cavity field due to the material loss in the metal is compensated by the growth

of the field due to gain of the material filling the cavity. In such a case, coupled-mode theory predicts that there is complete reflection and no transmission, and the device behaves essentially as if the metal were lossless. In general, we find that there is excellent agreement between the results of coupled-mode theory and FDFD simulations<sup>[18]</sup>.

For the side-coupled structure (inset of Fig. 4(a)), the InGaAsP medium filling the cavity is lossy ( $\epsilon_i = -0.1$ ) in the absence of pumping. In this case, we have  $1/\tau_0 - 1/\tau_g \gg 1/\tau_e$ , so there is very low reflection and high transmission at resonance. Figure 4(a) shows the transmission  $T$  and reflection  $R$  spectra of the device in the absence of pumping. We observe that an incident optical wave in the MDM plasmonic waveguide remains essentially undisturbed by the presence of the cavity. There is almost complete transmission of the incident optical wave through the MDM plasmonic waveguide ( $T \simeq 0.86$ ), while almost all the remaining portion of the incident optical power is absorbed in the cavity.

If the semiconductor material filling the cavity is pumped,  $\epsilon_i$  increases as a function of pump power and eventually becomes positive when the medium exhibits gain. In the presence of pumping, the transmission of an incident optical wave decreases. When the pumping is such that the material gain in the medium filling the cavity compensates the material loss in the metal ( $1/\tau_0 = 1/\tau_g$ ), the incident optical wave is completely reflected at resonance. For the side-coupled structure of Fig. 4(a), complete reflection is obtained for  $\epsilon_i \simeq 0.165$  which corresponds to a gain coefficient of  $g \simeq 2 \times 10^3 \text{ cm}^{-1}$ . Such a gain coefficient is within the limits of currently available semiconductor-based optical gain media<sup>[33,41,42]</sup>. Figure 4(b) shows the transmission  $T$  and reflection  $R$  spectra of the device for  $\epsilon_i = 0.165$ . We find that these spectra are very similar to those of the lossless metal case<sup>[18]</sup>. Note that, even though the MDM plasmonic waveguide is lossy, the propagation length of its fundamental propagating mode is much longer than the waveguide-cavity interaction length, which is approximately equal to the cavity length  $a$ . Thus, even though gain media are incorporated in only a selected device area, the device behaves as if the metal were lossless.

Thus, such a side-coupled structure in which the cavity is filled with a gain medium, can act as an extremely compact gain-assisted switch for MDM plasmonic waveguides, in which the on state corresponds to the absence of pumping of the semiconductor material filling the cavity, and the off state corresponds to pumping the material in the cavity with an intensity which compensates the material loss in the metal.

The switching time in such a device will be limited by the carrier lifetime which is on the order of  $0.2 \text{ ns}$ <sup>[41]</sup>. In addition, we estimate that the pumping power in the off state will be on the order of  $50 \mu\text{W}$ , by considering the required carrier density for gain coefficient<sup>[41]</sup> and assuming a device thickness of half a wavelength. Moreover, the device proposed here may also function as a plasmonic laser when the gain coefficient  $g$  reaches above  $2.16 \times 10^3 \text{ cm}^{-1}$ . At such a gain, the cavity loss, including both the material loss and coupling to the waveguide, is compensated by the gain.

## 6. Compact couplers between dielectric slab waveguides and MDM plasmonic waveguides

In MDM plasmonic waveguides, the propagation length of the fundamental subwavelength propagating mode is limited by material loss in the metal and is orders of tens of micrometers at frequencies around the optical communication wavelength ( $\lambda_0 = 1.55 \mu\text{m}$ )<sup>[9,43]</sup>. Thus for longer distances it is expected that conventional dielectric waveguides with diffraction-limited optical mode confinement will be used to carry the optical signal. The propagation length in dielectric waveguides is primarily limited by fabrication related disorders and is orders of magnitude larger than the propagation length of MDM plasmonic waveguides<sup>[44]</sup>. In short, it is expected that MDM waveguides will be used to address subwavelength optoelectronic devices, while conventional dielectric waveguides will be used to transfer the optical signal over distances longer than a few tens of microns. Couplers between MDM and dielectric waveguides will therefore be essential components for most applications involving the use of MDM waveguides such as optical interconnects. In this section, we investigate the coupling of high-index contrast dielectric slab waveguides to MDM plasmonic waveguides. Our focus here is on coupling structures either without any transition region between the dielectric and plasmonic waveguides, or with submicron scale transition regions. In previous studies, efficient coupling between dielectric and plasmonic waveguides has been demonstrated for a few microns long coupling regions<sup>[45–47]</sup>.

We define the transmission efficiency of the coupler  $T_{ij}$  as the ratio of the transmitted power into the fundamental mode of the output waveguide  $j$ , and of the incident power of the fundamental mode of the input waveguide  $i$ . We also note that due to reciprocity<sup>[27]</sup> the transmission efficiency from the dielectric to the plasmonic waveguide  $T_{dp}$  is equal to the transmission efficiency from the plasmonic to the dielectric waveguide  $T_{pd}$ .

We first consider a coupler created by simply placing an air-silicon-air dielectric slab waveguide terminated flat at the exit end of a silver-air-silver MDM plasmonic

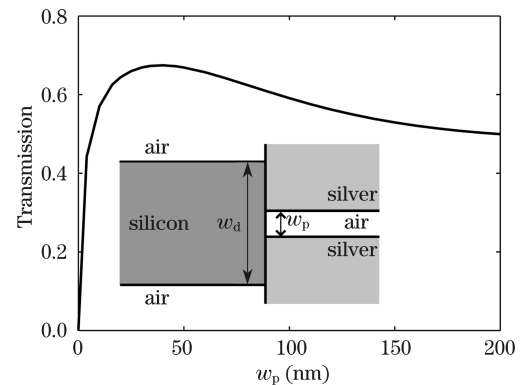


Fig. 5. Transmission efficiency of a coupler between a dielectric and a MDM waveguide as a function of the width of the plasmonic waveguide  $w_p$  at  $\lambda_0 = 1.55 \mu\text{m}$  calculated using FDFD. The coupler, created by placing the dielectric waveguide terminated flat at the exit end of the MDM waveguide, is shown in the inset. Results are shown for  $w_d = 300 \text{ nm}$ .

waveguide (inset of Fig. 5). Figure 5 shows the coupler transmission  $T_{dp}(=T_{pd})$  as a function of the width of the plasmonic waveguide  $w_p$  at  $\lambda_0 = 1.55 \mu\text{m}$ . The width of the dielectric waveguide is  $w_d = 300 \text{ nm}$ , which approximately corresponds to the optimal width of a silicon slab waveguide surrounded by air that achieves the minimum TM modal size. We observe that the transmission efficiency in this coupler is high and the maximum transmission of 68% is obtained for  $w_p \simeq 40 \text{ nm}$ . The transmission is also weakly dependent on  $w_p$  for  $w_p > 20 \text{ nm}$ . At the limit  $w_p \rightarrow 0$ , the transmission goes to zero as expected.

In general, we find that for a given width of the sub-wavelength MDM waveguide  $w_p$ , there is an optimum width of the dielectric waveguide  $w_d$  which maximizes the transmission efficiency and *vice versa*. We also find that for a given  $w_d$  the optimum  $w_p$  is significantly smaller than  $w_d$ . This is due to the fact that a subwavelength MDM waveguide collects light from an area significantly larger than its cross-sectional area<sup>[48]</sup>. More precisely, the transmission cross section of a MDM waveguide (in the unit of length in two dimensions), defined as the transmitted power into the waveguide normalized by the incident plane wave power flux, is significantly larger than its geometric cross-sectional area. As an example, the transmission cross section of a MDM waveguide with  $w_p = 50 \text{ nm}$  is  $\sim 185 \text{ nm}$  at  $\lambda_0 = 1.55 \mu\text{m}$ . On the other hand, the transmission cross section of dielectric waveguides is approximately equal to their geometrical area. For example, for a waveguide consisting of a silicon slab surrounded by air with  $w_d = 320 \text{ nm}$ , the transmission cross section is  $\sim 340 \text{ nm}$  at  $\lambda_0 = 1.55 \mu\text{m}$ .

To further increase the transmission, we design a coupler consisting of a multisection taper shown in Fig. 6(a). Such tapers, consisting of a number of waveguide sections, have been used as couplers between dielectric waveguides with highly different widths<sup>[49–51]</sup>. It has been shown theoretically and confirmed experimentally that they can be designed to have higher transmission efficiency than conventional tapers of the same length with linear or parabolic shapes<sup>[50,51]</sup>. The coupler design used here consists of a number of dielectric waveguide and MDM waveguide sections. The widths of these sections are optimized using a genetic global optimization algorithm in combination with FDFD. More specifically, we use a microgenetic algorithm which has been shown to reach the near-optimal region much faster than large population genetic algorithms<sup>[52,53]</sup>. Using this approach, we designed a coupler with 93% transmission efficiency for  $w_d = 300 \text{ nm}$  and  $w_p = 50 \text{ nm}$  at  $\lambda_0 = 1.55 \mu\text{m}$ . In this design we use 4 dielectric waveguide sections and 4 MDM waveguide sections. The lengths of all waveguide sections are  $l_i = 50 \text{ nm}$ . Their widths  $w_1, w_2, \dots, w_8$  are optimized using the microgenetic algorithm, while the number of dielectric and MDM sections as well as their lengths are kept fixed during the optimization process. The designed coupler is extremely compact with a total length of  $400 \text{ nm}$ .

Both the simple coupler of Fig. 5 and the multisection taper of Fig. 6(a) were optimized at a single wavelength of  $\lambda_0 = 1.55 \mu\text{m}$ . Figure 6(b) shows the transmission efficiency of these couplers as a function of wavelength. We observe that in both cases the transmission efficiency

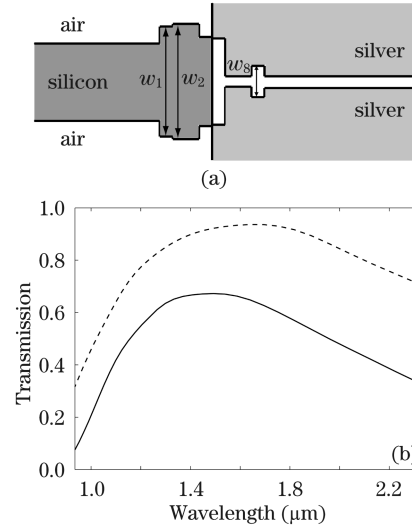


Fig. 6. (a) Schematic of a coupler consisting of a multisection taper. (b) Transmission efficiency as a function of wavelength for the couplers of Fig. 5 (solid line) and Fig. 6(a) (dashed line). In both cases the coupler parameters are optimized at  $\lambda_0 = 1.55 \mu\text{m}$ .

is close to its maximum value in a broad range of wavelengths. This is due to the fact that in both cases the high transmission efficiency is not associated with any strong resonances. Similar broadband responses are observed in couplers between dielectric waveguides with highly different widths based on multisection tapers<sup>[50,51]</sup> and in multisection impedance matching transformers used in microwave circuits<sup>[27]</sup>.

## 7. Conclusions

In summary, we first showed that, even though MDM plasmonic waveguides are lossy, bends and splitters with no additional loss can be designed over a very broad wavelength range that extends from DC to near-infrared, if the waveguide width  $d$  is small enough. We note that this remarkable effect is not observed in other light-guiding structures such as high-index contrast or photonic crystal waveguides. We also introduced mode converters with no additional loss which couple MDM plasmonic waveguides with different widths.

In addition, we demonstrated that optical gain provides a mechanism for on/off switching in MDM plasmonic waveguides. The proposed extremely compact gain-assisted plasmonic switch consists of a MDM plasmonic waveguide side-coupled to a cavity filled with a semiconductor gain material. The on state corresponds to the absence of pumping of the semiconductor material filling the cavity, and the off state corresponds to pumping the material in the cavity with an intensity which compensates the material loss in the metal. The required gain coefficients are within the limits of currently available semiconductor-based optical gain media.

Finally, we showed that, despite the large difference between the modal sizes of dielectric and MDM plasmonic waveguides, a simple coupler created by placing the dielectric waveguide terminated flat at the exit end of the MDM waveguide without any tapering could be designed to have a transmission efficiency of  $\sim 70\%$  at the optical communication wavelength. We also showed

that the transmission efficiency of the coupler could be increased to 93% by using a 400-nm-long multisection taper. In both cases the transmission was found to be broadband.

### Acknowledgement

This research was supported by DARPA/MARCO under the Interconnect Focus Center and by AFOSR grant FA 9550-04-1-0437.

### References

- J. Takahara, S. Yamagishi, H. Taki, A. Morimoto, and T. Kobayashi, *Opt. Lett.* **22**, 475 (1997).
- J.-C. Weeber, A. Dereux, C. Girard, J. R. Krenn, and J.-P. Goujonnet, *Phys. Rev. B* **60**, 9061 (1999).
- J. R. Krenn, B. Lamprecht, H. Ditlbacher, G. Schider, M. Salerno, A. Leitner, and F. R. Aussenegg, *Europhys. Lett.* **60**, 663 (2002).
- M. L. Brongersma, J. W. Hartman, and H. A. Atwater, *Phys. Rev. B* **62**, R16356 (2000).
- S. A. Maier, P. G. Kik, H. A. Atwater, S. Meltzer, E. Harel, B. E. Koel, and A. A. G. Requicha, *Nature Mater.* **2**, 229 (2003).
- K. Tanaka and M. Tanaka, *Appl. Phys. Lett.* **82**, 1158 (2003).
- V. R. Almeida, Q. Xu, C. A. Barrios, and M. Lipson, *Opt. Lett.* **29**, 1209 (2004).
- E. N. Economou, *Phys. Rev.* **182**, 539 (1969).
- R. Zia, M. D. Selker, P. B. Catrysse, and M. L. Brongersma, *J. Opt. Soc. Am. A* **21**, 2442 (2004).
- J. A. Dionne, L. A. Sweatlock, H. A. Atwater, and A. Polman, *Phys. Rev. B* **72**, 075405 (2005).
- J. A. Dionne, L. A. Sweatlock, H. A. Atwater, and A. Polman, *Phys. Rev. B* **73**, 035407 (2006).
- Ş. E. Kocabaş, G. Veronis, D. A. B. Miller, and S. Fan, *Phys. Rev. B* **79**, 035120 (2009).
- J. A. Dionne, H. J. Lezec, and H. A. Atwater, *Nano Lett.* **6**, 1928 (2006).
- H. J. Lezec, J. A. Dionne, and H. A. Atwater, *Science* **316**, 430 (2007).
- E. Verhagen, J. A. Dionne, L. K. Kuipers, H. A. Atwater, and A. Polman, *Nano Lett.* **8**, 2925 (2008).
- G. Veronis and S. Fan, *Appl. Phys. Lett.* **87**, 131102 (2005).
- Ş. E. Kocabaş, G. Veronis, D. A. B. Miller, and S. Fan, *IEEE J. Sel. Top. Quantum Electron.* **14**, 1462 (2008).
- Z. Yu, G. Veronis, S. Fan, and M. L. Brongersma, *Appl. Phys. Lett.* **92**, 041117 (2008).
- G. Veronis and S. Fan, *Opt. Express* **15**, 1211 (2007).
- S.-D. Wu and E. N. Glytsis, *J. Opt. Soc. Am. A* **19**, 2018 (2002).
- G. Veronis, R. W. Dutton, and S. Fan, *Opt. Lett.* **29**, 2288 (2004).
- E. D. Palik, *Handbook of Optical Constants of Solids* (Academic, Orlando, 1985).
- J. Jin, *The Finite Element Method in Electromagnetics* (Wiley, New York, 2002).
- A. Taflov and S. C. Hagness, *Computational Electrodynamics* (3rd edn.) (Artech House, Boston, 2005).
- C. Manolatou, S. G. Johnson, S. Fan, P. R. Villeneuve, H. A. Haus, and J. D. Joannopoulos, *J. Lightwave Technol.* **17**, 1682 (1999).
- S. Ramo, J. R. Whinnery, and T. V. Van Duzer, *Fields and Waves in Communication Electronics* (3rd edn.) (Wiley, New York, 1994).
- D. M. Pozar, *Microwave Engineering* (2nd edn.) (Wiley, New York, 1998).
- R. E. Collin, *Foundations for Microwave Engineering* (McGraw-Hill, New York, 1966).
- D. J. Bergman and M. I. Stockman, *Phys. Rev. Lett.* **90**, 027402 (2003).
- N. M. Lawandy, *Appl. Phys. Lett.* **85**, 5040 (2004).
- J. Seidel, S. Grafström, and L. Eng, *Phys. Rev. Lett.* **94**, 177401 (2005).
- M. A. Noginov, G. Zhu, M. Bahoura, J. Adegoke, C. E. Small, B. A. Ritzo, V. P. Drachev, and V. M. Shalaev, *Opt. Lett.* **31**, 3022 (2006).
- M. P. Nezhad, K. Tetz, and Y. Fainman, *Opt. Express* **12**, 4072 (2004).
- S. A. Maier, *Opt. Commun.* **258**, 295 (2006).
- D. S. Citrin, *Opt. Lett.* **31**, 98 (2006).
- S. A. Ramakrishna and J. B. Pendry, *Phys. Rev. B* **67**, 201101 (2003).
- A. A. Govyadinov and V. A. Podolskiy, *Phys. Rev. Lett.* **97**, 223902 (2006).
- S. Xiao, L. Liu, and M. Qiu, *Opt. Express* **14**, 2932 (2006).
- A. Hosseini and Y. Massoud, *Appl. Phys. Lett.* **90**, 181102 (2007).
- H. A. Haus and Y. Lai, *IEEE J. Quantum Electron.* **28**, 205 (1992).
- T. Saitoh and T. Mukai, *IEEE J. Quantum Electron.* **23**, 1010 (1987).
- N. Kirstaedter, O. G. Schmidt, N. N. Ledentsov, D. Bimberg, V. M. Ustinov, A. Yu. Egorov, A. E. Zhukov, M. V. Maximov, P. S. Kop'ev, and Zh. I. Alferov, *Appl. Phys. Lett.* **69**, 1226 (1996).
- G. Veronis and S. Fan, *Opt. Lett.* **30**, 3359 (2005).
- M. Lipson, *J. Lightwave Technol.* **23**, 4222 (2005).
- P. Ginzburg, D. Arbel, and M. Orenstein, *Opt. Lett.* **31**, 3288 (2006).
- L. Chen, J. Shakya, and M. Lipson, *Opt. Lett.* **31**, 2133 (2006).
- M. Hochberg, T. Baehr-Jones, C. Walker, and A. Scherer, *Opt. Express* **12**, 5481 (2004).
- H. Henke, H. Früchtling, and R. Winz, *Radio Sci.* **14**, 11 (1979).
- M. M. Spuhler, B. J. Offrein, G.-L. Bona, R. Germann, I. Massarek, and D. Erni, *J. Lightwave Technol.* **16**, 1680 (1998).
- B. Luyssaert, P. Vandersteegen, D. Taillaert, P. Dumon, W. Bogaerts, P. Bienstman, D. V. Thourhout, V. Wiaux, S. Beckx, and R. Baets, *IEEE Photon. Technol. Lett.* **17**, 73 (2005).
- B. Luyssaert, P. Bienstman, P. Vandersteegen, P. Dumon, and R. Baets, *J. Lightwave Technol.* **23**, 2462 (2005).
- K. Krishnakumar, *Proc. SPIE* **1196**, 289 (1990).
- B. Wang, J. Jiang, and G. P. Nordin, *Opt. Express* **12**, 3313 (2004).